Theoretical study of the ordered-vacancy semiconducting compound $CdAl_2Se_4$

2001 J. Phys.: Condens. Matter 13 1669

(http://iopscience.iop.org/0953-8984/13/8/305)

INSTITUTE OF PHYSICS PUBLISHING JOURNAL OF PHYSICS: CONDENSED MATTER

J. Phys.: Condens. Matter **13** (2001) 1669–1684 www.iop.org/Journals/cm PII: S0953-8984(01)15822-4

Theoretical study of the ordered-vacancy semiconducting compound $CdAl_2Se_4$

Miguel Fuentes-Cabrera and Otto F Sankey

Department of Physics and Astronomy and Materials Research Centre, Arizona State University, Tempe, AZ 85287, USA

Received 26 July 2000, in final form 27 October 2000

Abstract

We report results from first-principles density functional calculations of the structural, electronic, and vibrational properties of the semiconducting $CdAl_2Se_4$ compound. The defective chalcopyrite-like $I\bar{4}$ phase and the spinel-like $Fd\bar{3}m$ phases are considered. We find within the local density approximation (LDA) that the total energies of the $I\bar{4}$ and the $Fd\bar{3}m$ phases are virtually identical. Within the generalized gradient approximation, however, the ground-state structure is found to be $I\bar{4}$ (in agreement with experiment), while the $Fd\bar{3}m$ phase is a high-pressure phase that theoretically becomes stable at 3 GPa (4.5 GPa experimentally). The $I\bar{4}$ phase is found to have a direct electronic band gap while the $Fd\bar{3}m$ phase has an indirect band gap. A correction of the LDA band gap for $I\bar{4}$ using a generalized density functional theory is in excellent agreement with measurements. The vibrational spectrum of the $I\bar{4}$ structure at zero pressure and as a function of pressure is determined. Up to 23 GPa, no modes become soft.

1. Introduction

The ordered-vacancy compounds $A^{II}B_2^{III}C_4^{VI}$ are a class of materials with technological interest due to their semiconducting properties, broad band gaps, and potential applications in nonlinear optical and photovoltaic devices. Despite this, not many of these materials have been studied by modern electronic structure methods. The crystal structures of the ordered-vacancy compounds can be considered derivatives of the zinc-blende structure. Like zinc-blende structure, they are tetrahedrally bonded frameworks if one considers a vacancy in each unit cell as an *extra atom with zero valence* [1, 2]. The understanding of the role played by vacancies in bonding and in the pressure-induced transitions has attracted much theoretical and experimental attention. This motivated the theoretical work of Bernard and Zunger [3] and Marinelli *et al* [4], who investigated the chemical bonding in $CdIn_2Se_4$ by means of a first-principles technique, and the recent experimental work of Ursaki *et al* [5], who measured the vibrational spectra under pressure of AGa_2X_4 (A = Cd, Zn; X = S, Se) compounds.

$CdAl_2Se_4$ is an interesting ordered-vacancy compound, of which many experimental studies exist. It is known from the early work of Hahn *et al* [6] that the structure of $CdAl_2Se_4$

0953-8984/01/081669+16$30.00

is $I\bar{4}$. Later Range *et al* [7] observed a phase change to spinel structure at 4.5 GPa and 400 °C. Recently, several experimental studies have been performed to determine its optical and vibrational properties at zero pressure [8–11]. To our knowledge a theoretical study of all of these properties has not yet been undertaken.

It is the purpose of this paper to study the energetics, and the electronic and vibrational properties of $CdAl_2Se_4$ by means of an *ab initio* electronic structure technique. We have considered for this study the two phases observed experimentally: $I\bar{4}$ and spinel-like $Fd\bar{3}m$.

2. Optimized structures

First we describe the two phases, $I\bar{4}$ and $Fd\bar{3}m$, that we consider for $CdAl_2Se_4$. The $I\bar{4}$ phase is shown in figure 1(a). The structure is a defective chalcopyrite-like body-centred-tetragonal lattice which contains seven atoms and one vacancy per unit cell. If we consider the vacancy as an 'atom', each atom is surrounded by four neighbours in a tetrahedral-like configuration. The Cd, Al, and vacancies are each surrounded by four Se atoms, while the Se atoms are surrounded by two Al, one Cd, and one vacancy.

The spinel-like $Fd\bar{3}m$ phase is represented in figure 1(b). The unit cell is cubic and contains 14 atoms, $(CdAl_2Se_4)_2$. The coordination of the atoms in this phase is no longer tetrahedral. Each Cd is tetrahedrally coordinated by four Se atoms, and each Se is tetrahedrally coordinated by three Al and one Cd, but each Al is surrounded by six Se. In the namesake mineral spinel, $MgAl_2O_4$, it is Al that is octahedrally coordinated by oxygen.

We use density functional theory (DFT) in the local density approximation (LDA) and generalized gradient approximation (GGA) to determine the equilibrium internal and external coordinates, and the equations of state (EOS). This method used pseudopotentials in a plane-wave expansion of the eigenstates. All of the calculations were carried out using the Vienna *ab initio* simulation package (VASP) [12], and used soft Vanderbilt-type pseudopotentials [13, 14] which included as valence states the outermost d electrons of the Cd atoms. For the LDA, we use the Ceperley–Alder [15] expression for the exchange–correlation energy as parametrized by Perdew and Zunger [16]. For the GGA, we use the Perdew and Wang [17] expression. Integrations over the Brillouin zone were carried out using the Monkhorst–Pack scheme [18]. Tests were performed to ensure that convergence was reached with the number of plane waves used and in the Brillouin zone sampling. For the $I\bar{4}$ phase, we find that the energy is well converged with an energy cut-off of 12.34 Ryd and 12 k-points. For the spinel-like $Fd\bar{3}m$ phase, we also find that an energy cut-off of 12.34 Ryd is sufficient, and that ten irreducible k-points leads to a well converged total energy. Both structures yielded insulators.

The optimized internal coordinates and unit-cell parameters are obtained by a conjugate gradient energy-minimization procedure. This procedure simultaneously optimizes both the cell parameters and the internal positions of the atoms. The internal fractional coordinates of the optimized structures for the $I\bar{4}$ and the $Fd\bar{3}m$ structures are summarized in table 1. The optimized lattice parameters are in table 2. Experimental results are also listed in tables 1 and 2.

A comparison of theoretical and experimental lattice parameters (table 2) shows that the LDA approximation underestimates them while the GGA overestimates them. The LDA values are 0.1–1.6% shorter than experimental ones, while the GGA values are 1.7–2.7% larger. The agreement between the theoretical LDA and experimental values of Hahn *et al* [6] is satisfactory. It is also similar to the agreement with experiment obtained by Bernard and Zunger [3] and Marinelli *et al* [4] for $CdIn_2Se_4$. We will use the LDA-relaxed structures for studying the electronic and the vibrational properties of $CdAl_2Se_4$.

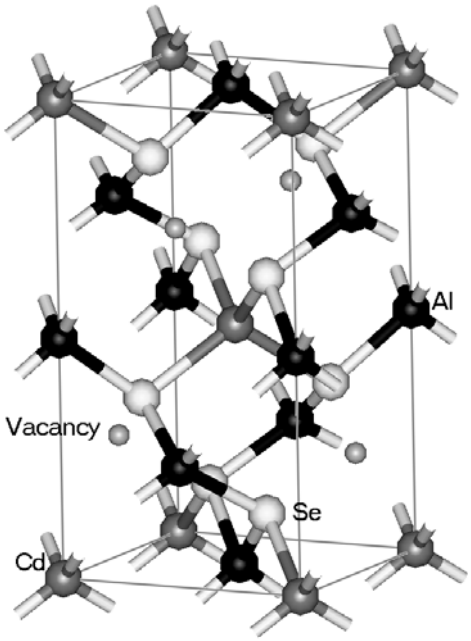

(a)

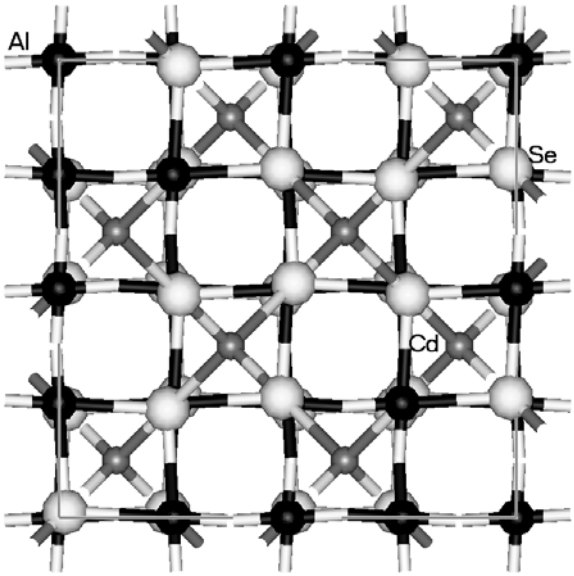

(b)

Figure 1. The structures studied: (a) chalcopyrite-like $I\bar{4}$; (b) spinel-like $Fd\bar{3}m$.

An EOS is obtained by fitting the *ab initio* total energy versus volume curve to a Birch–Murnaghan equation of state [19]. Figure 2 shows the fitted equation of state for each structure relaxed using the LDA and the GGA. The parameters extracted from this fitting are listed in table 3. The parameters are the minimum energy E_0, the equilibrium volume V_0, the bulk modulus K, and the pressure derivative of the bulk modulus K'.

Table 1. The LDA- and GGA-optimized internal coordinates of the $I\bar{4}$ and $Fd\bar{3}m$ phases.

$I\bar{4}$		$Fd\bar{3}m$	
Element	Site	Element	Site
Cd	2a (0, 0, 0); etc	Cd	8a ($\frac{1}{8}$, $\frac{1}{8}$, $\frac{1}{8}$); etc
Al	2b (0, 0, $\frac{1}{2}$); etc	Al	16d ($\frac{1}{2}$, $\frac{1}{2}$, $\frac{1}{2}$); etc
Al	2c (0, $\frac{1}{2}$, $\frac{1}{4}$); etc		
Vacancy	2d (0, $\frac{1}{2}$, $\frac{3}{4}$); etc		
Se	8g (x, y, z); etc	Se	32e (x, x, x); etc
	LDA, (x, y, z) = (0.276, 0.259, 0.140)		LDA, $x = 0.263$
	GGA, (x, y, z) = (0.270, 0.269, 0.137)		GGA, $x = 0.264$
	Experiment [8], (x, y, z) = (0.2686, 0.267, 0.1366)		
	Experiment [6], (x, y, z) = (0.27, 0.27, 0.136)		

Table 2. The optimal external parameters obtained with a LDA and GGA calculation. Experimental values are also presented where available. GGA values are in parentheses.

Phase	a_0 (Å)	c_0 (Å)	c_0/a_0	Volume (Å^3)
$I\bar{4}$	5.67 (5.86)	10.59 (10.89)	1.86 (1.86)	340.46 (374)
Experiment [8]	5.76	10.71	1.86	355.33
Experiment [6]	5.73	10.6	1.85	348.03
$Fd\bar{3}m$	10.73 (10.97)			1235.38 (1320.14)
Experiment [7]	10.77			1249.24

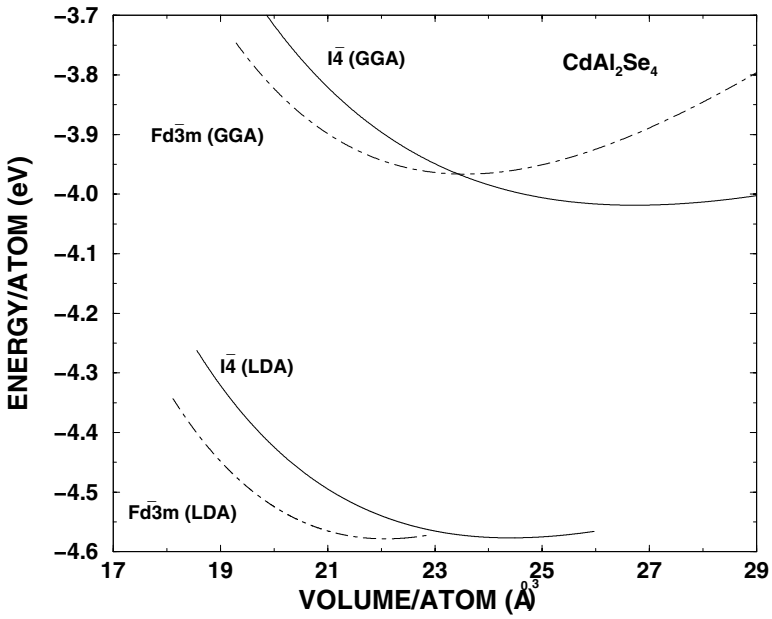

Figure 2. Equations of state (energy per atom versus volume per atom) for the $I\bar{4}$ and spinel-like $Fd\bar{3}m$ phases. The data in the plot were obtained from a Birch–Murnaghan fit to the LDA and GGA calculations. Table 3 summarizes the Birch–Murnaghan parameters.

Table 3. The parameters of the Birch–Murnaghan equation of state obtained from a fit of the LDA and GGA energy versus volume data. GGA values are in parentheses.

Phase	E_0 (eV/atom)	V_0 (volume/atom)	K (GPa)	K'
$I\bar{4}$	−4.577 (−4.019)	24.404 (26.724)	40.100 (31.479)	5.395 (5.143)
$Fd\bar{3}m$	−4.578 (−3.967)	22.073 (23.557)	74.336 (63.063)	4.394 (4.512)

Figure 2 shows that, within the LDA approximation, the $I\bar{4}$ and the $Fd\bar{3}m$ phases have virtually the same energy. The GGA, also shown in figure 2, is required to obtain the correct energy ordering of the two phases. The GGA result finds that the $I\bar{4}$ phase is more stable than the $Fd\bar{3}m$ phase, in agreement with experiments. The fact that the GGA is in better agreement with experiment than the LDA is consistent with the fact that a vacancy compound will have larger variations of the electron density, which are more accurately accounted for with a model that includes gradient corrections.

To determine the pressure at the transition from the $I\bar{4}$ to the $Fd\bar{3}m$ structure we have calculated the enthalpy $(E + PV)$ of each structure within the GGA, and plotted the results versus the pressure. In this analysis, we are assuming very low temperature, so the Gibbs energy, $G = E + PV - TS$, reduces to just the enthalpy. The state of lowest enthalpy at a given pressure is the predicted phase at that pressure. The results are shown in figure 3. It is seen that the transition from the $I\bar{4}$ defective-chalcopyrite structure to the $Fd\bar{3}m$ spinel-like structure occurs at 3 GPa. This is in qualitative agreement with experiment. Experimentally, this transition has been found at 4.5 GPa and 400 °C [7].

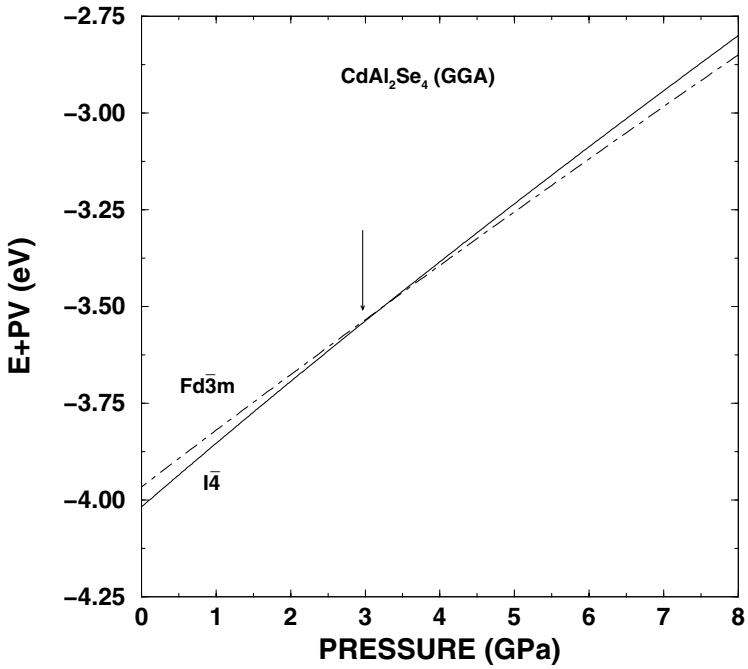

Figure 3. $E + PV$, for the $I\bar{4}$ and spinel-like $Fd\bar{3}m$ phases. The data in the plot were obtained from a Birch–Murnaghan fit of the GGA calculation.

3. Electronic properties

Significant motivation for studying the ordered-vacancy semiconductors is provided by their electronic properties. Basic questions remain concerning this issue for $CdAl_2Se_4$. The optical properties of the $I\bar{4}$ phase have been measured, and this gives some clues to the electronic states of the material. However, a detailed description of the transitions has not been determined. In the spinel-like high-pressure phase, there have been no measurements related to its band structure.

3.1. Band structures calculated with the local density approximation (LDA)

3.1.1. $I\bar{4}$ phase. The band structure of the LDA-relaxed $I\bar{4}$ phase is shown in figure 4(a). The top of the valence band is at zero energy. We find that this phase has a direct band gap of 2.05 eV at the Γ ($\vec{k} = \vec{0}$) point. The band gap determined experimentally [9] is 2.95 eV, although it has not yet been clarified whether the band gap is direct or indirect.

The valence band region of the band structure is 13 eV wide, and it is divided into three sets that we will call low-, intermediate-, and higher-energy sets of bands. We have analysed the contribution of the anion and cations states to each set of bands by decomposing the total density of states (DOS) into s-, p-, and d-orbital contributions. The result is the site-projected partial density of states shown in figures 5(a), 5(b), 5(c), 5(d) (the corresponding one for the $Fd\bar{3}m$ phase is shown in figure 6; see the next section). There is not just one way to perform this atom and orbital decomposition, so the results should be interpreted qualitatively. Clearly, the low-energy set of valence bands are derived from Se s orbitals with a small contribution from Cd d orbitals. The intermediate-energy set of valence bands are derived from the semi-core Cd d orbitals. The higher-energy set of valence bands can be further divided into two subbands. The lower-energy subband from -5.5 to -3.2 eV is an Al s and Se p band. The higher-energy subband from -3.2 to 0.0 eV is a Se p band with a small contribution from the Al p, Cd d, and Cd s orbitals. Finally, the total DOS is shown in figure 7(a).

The pressure dependence of the band gap, E_g, of the $I\bar{4}$ phase was also examined. The results are shown in figure 8. It is clear that at 6 GPa the band gap reaches a maximum with a value of 2.25 eV. We find that the band gap is direct and at the Γ point until 3.96 GPa is reached. For higher pressures, the band gap becomes indirect; the top of the valence band remains at the Γ point but the location of the conduction band minimum changes with pressure. The bottom of the conduction band is along the $Z((2\pi/a)(0, 0, a/c))$–Γ direction at pressures from 5.2 to 10.1 GPa, while at pressures from 10.1 to 22.6 GPa it is located at the X point, $(2\pi/a)(1, 0, 0)$.

3.1.2. $Fd\bar{3}m$ phase. The band structure of the geometrically LDA-optimized $Fd\bar{3}m$ phase is shown figure 4(b). We find that this phase is semiconducting with an indirect band gap of 1.47 eV, with the top of the valence band along the $K((2\pi/a)(\frac{3}{4}, \frac{3}{4}, 0))$–$\Gamma$ line, the bottom of the conduction band being at the Γ ($\vec{k} = \vec{0}$) point. We are not aware of any previous results concerning the electronic properties of the spinel-like phase of $CdAl_2Se_4$.

The valence band part of the band structure of the $Fd\bar{3}m$ phase is 13.8 eV wide and it is also divided into three regions. We show the site-projected partial density of states in figures 6(a), 6(b), 6(c). It is interesting to observe that the contributions of the anion and cation states to each set of bands are of a similar character to those found for the $I\bar{4}$ phase. The total DOS is shown in figure 7(b).

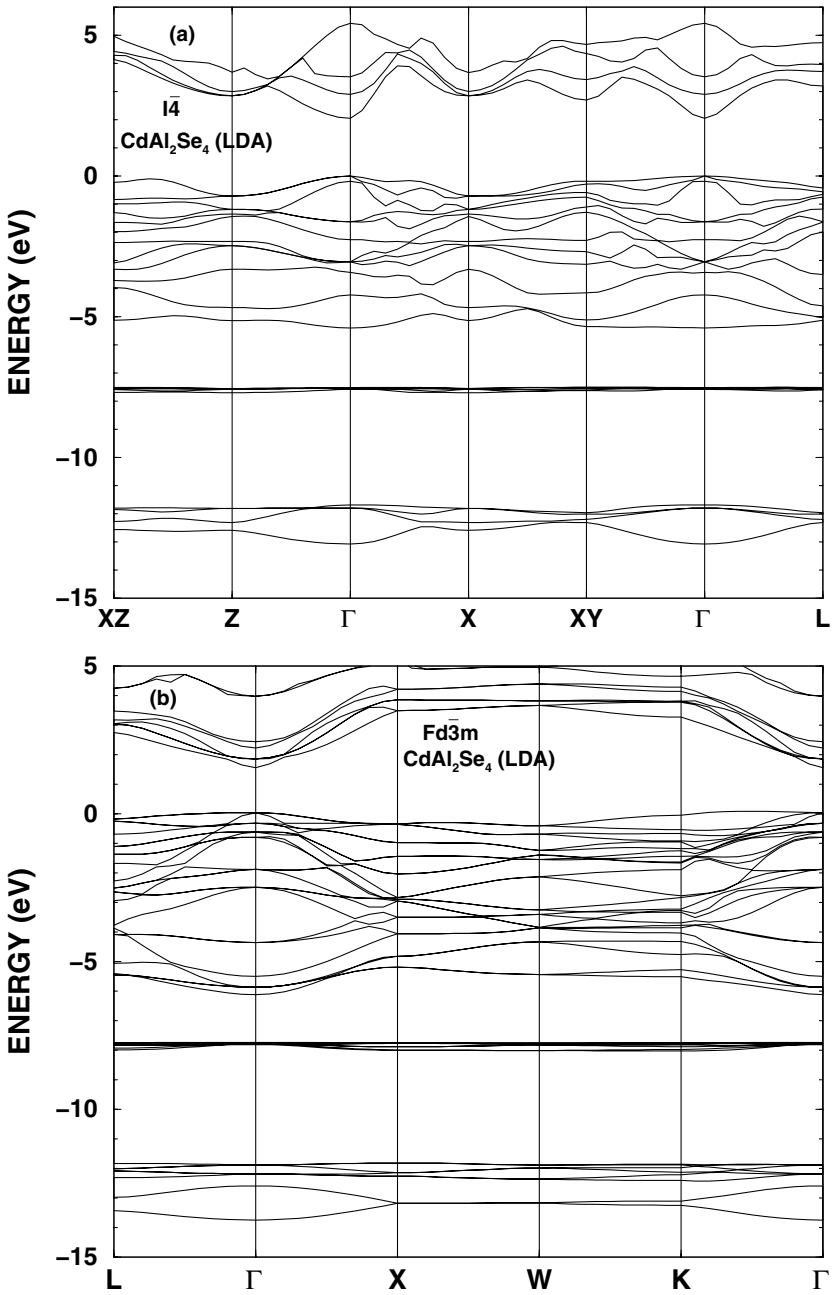

Figure 4. The LDA band structures of the equilibrium volumes V_0 of each phase (see table 2) obtained by a LDA calculation. The top of the valence band is at 0.0 eV. (a) The $I\bar{4}$ phase. The high-symmetry points are XZ $= (\pi/a)(1, 0, a/c)$, Z $= (2\pi/a)(0, 0, a/c)$, $\Gamma = (0, 0, 0)$, X $= (2\pi/a)(1, 0, 0)$, XY $= (\pi/a)(1, 1, 0)$, and L $= (\pi/a)(1, 1, a/c)$. (b) The spinel-like $Fd\bar{3}m$ phase. The high-symmetry points are L $= (2\pi/a)(\frac{1}{2}, \frac{1}{2}, \frac{1}{2})$, $\Gamma = (0, 0, 0)$, X $= (2\pi/a)(1, 0, 0)$, W $= (2\pi/a)(1, \frac{1}{2}, 0)$, and K $= (2\pi/a)(\frac{3}{4}, \frac{3}{4}, 0)$.

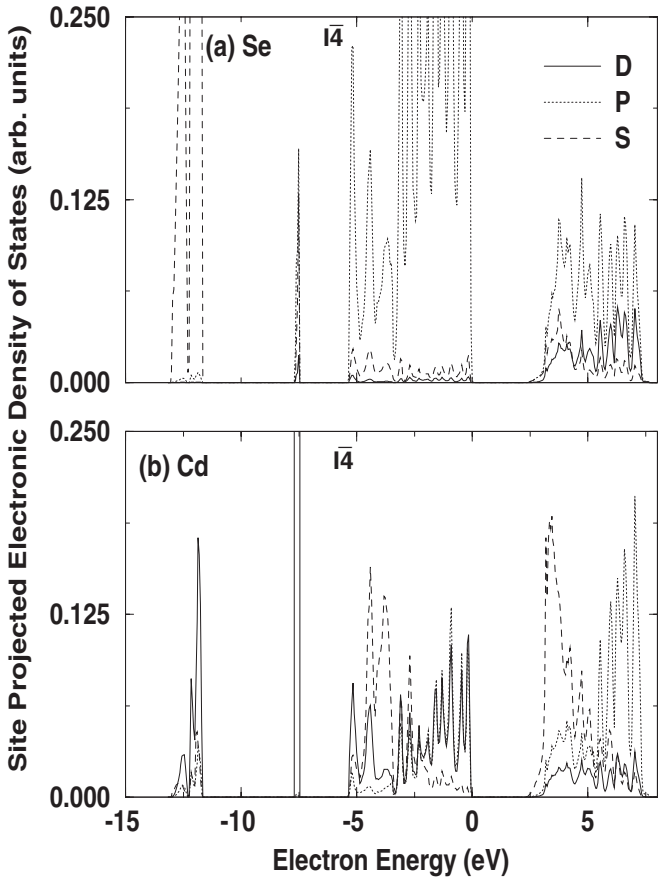

Figure 5. The LDA site-projected partial electronic density of states of the geometrically LDA-optimized $I\bar{4}$ phase at (a) the Se site, (b) the Cd site, (c) the Al site at 2c, and (d) the Al site at 2b. The solid, dotted, and dashed lines represent the d orbital, p orbital, and s orbital, respectively. The top of the valence band is at 0.0 eV.

3.2. Generalized density functional theory correction to the LDA band gaps

It is well known that LDA typically underestimates the band gap. To improve the LDA band gaps we have used the generalized density functional theory (GDFT) [20]. For this theory there are several levels of approximation. We have chosen the first level in which the correction to the band gap is given by the simple expression

$$\Delta_{cv} = \int [2\epsilon_{xc}(n_0(\vec{r})) - \mu_{xc}(n_0(\vec{r}))](|\psi_c(\vec{r})|^2 - |\psi_v(\vec{r})|^2)\, \mathrm{d}^3 r. \tag{1}$$

Here Δ_{cv} is the energy correction to the gap separating the conduction and valence electron states (ψ_c and ψ_v respectively), and ϵ_{xc} and μ_{xc} are the LDA exchange/correlation energy and potentials, respectively. The physical meaning of equation (1) is that the total energy difference between the ground state and the excited state with an electron–hole pair is not given just by a difference of electron energy eigenvalues; also one must compute all contributions to the total energy which also includes changes of the charge density δn ($\delta n(\vec{r}) = |\psi_c(\vec{r})|^2 - |\psi_v(\vec{r})|^2$). A further approximation involved is that the electron–electron correlation function $f(\vec{r}', \vec{r})$, is unaltered in the excited state containing the electron and hole.

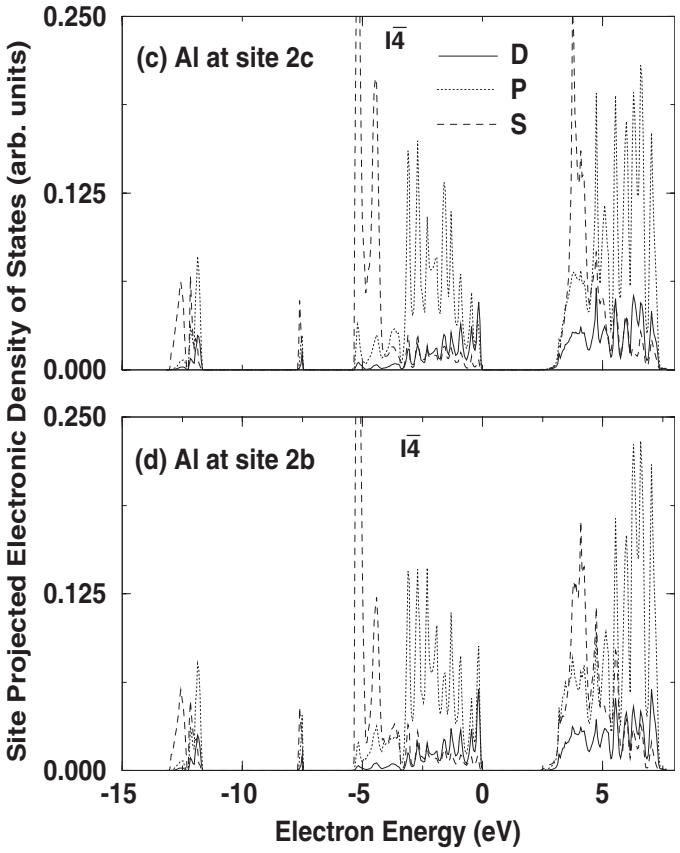

Figure 5. (Continued)

Equation (1) has been applied to correct the band gap of a variety of systems with remarkable success [20, 21]. It has also been applied to correct the band gap of the β-phase and spinel or γ-phase of Ge_3N_4 [22]. To our knowledge this is the first time the GDFT approximation has been used to correct the LDA band gap of a defective-tetrahedral compound. The results that we have obtained are shown in figures 9(a), 9(b) for the $I\bar{4}$ and $Fd\bar{3}m$ phases, respectively. The conduction band states have been corrected in both cases by considering the hole $|\psi_v|^2$ in equation (1) to be located at the valence band maximum.

In figure 9(a) it is seen that the GDFT correction opens up the LDA band gap of the $I\bar{4}$ phase. The 2.05 eV gap obtained using the LDA now opens up to 3.1 eV with GDFT. This is in excellent agreement with the 2.95 eV measured value [9]. The band gap remains direct and is located at the Γ ($\vec{k} = \vec{0}$) point. In figure 9(b) it is seen that the GDFT also opens the band gap of the $Fd\bar{3}m$ phase. The 1.47 eV gap obtained with LDA is opened to 2.28 eV. It remains indirect, with the top of the valence band along the K$((2\pi/a)(\frac{3}{4}, \frac{3}{4}, 0))$–$\Gamma$ line and the bottom of the conduction band at the Γ ($\vec{k} = \vec{0}$) point.

4. Vibrational properties

The vibrational modes of a material at the Γ point ($\vec{k} = \vec{0}$) of the phonon dispersion curves are especially important because they can be measured in Raman and infrared experiments.

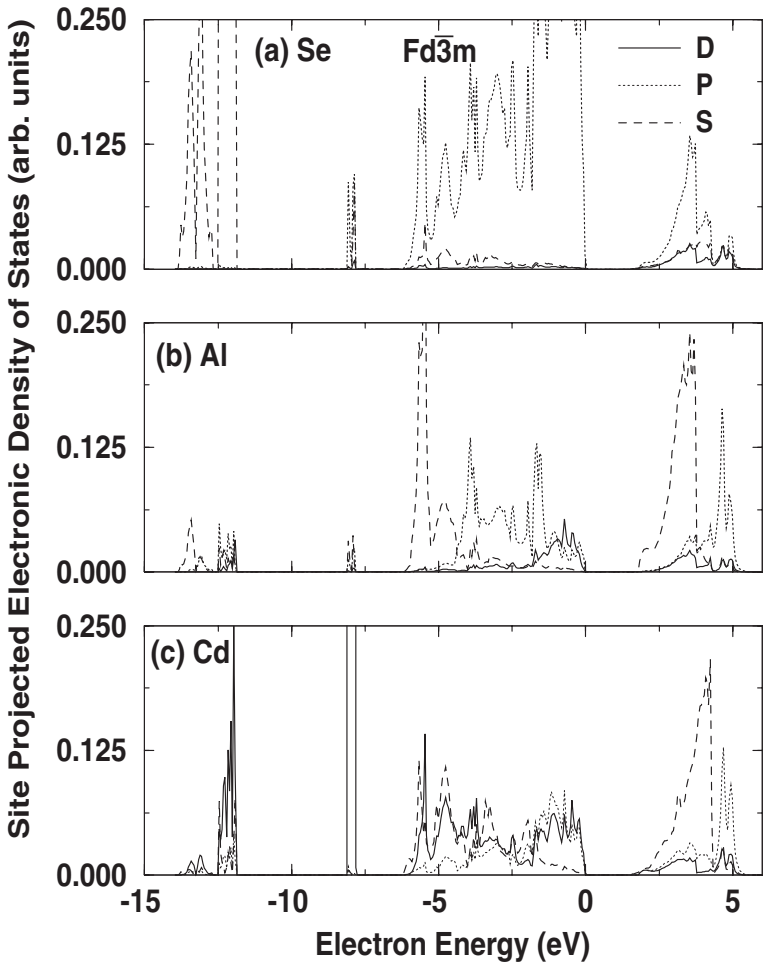

Figure 6. The LDA site-projected partial electronic density of states of the geometrically LDA-optimized $Fd\bar{3}m$ phase at (a) the Se site, (b) the Al site, (c) the Cd site. The solid, dotted, and dashed lines represent the d orbital, p orbital, and s orbital, respectively. The top of the valence band is at 0.0 eV.

Analyses of these spectra are useful in identifying phases and their properties and, if the pressure dependence of the spectra is analysed, provide information on the phase stability and on pressure-induced transitions. In this section, we present results on the vibrational properties of the $I\bar{4}$ phase. We have calculated the vibrational spectrum of this phase at the Γ point at zero pressure and have compared it with experimental results. The pressure dependence of the vibrational spectra is also examined. To our knowledge, there have been neither theoretical nor experimental studies that have analysed the pressure dependence of the vibrational spectra of $CdAl_2Se_4$.

The vibrational modes were determined from the force-constant matrix. The force-constant matrix was obtained by means of a first-principles electronic structure approach [23, 24]. In this approach, we began with the static equilibrium structure and displaced a *single* atom by a small displacement U_0 in a specific direction. We have used 11 independent displacements, each of magnitude U_0, which were in the directions $\vec{x}$, $\vec{y}$, and $\vec{z}$ for the Al(2b),

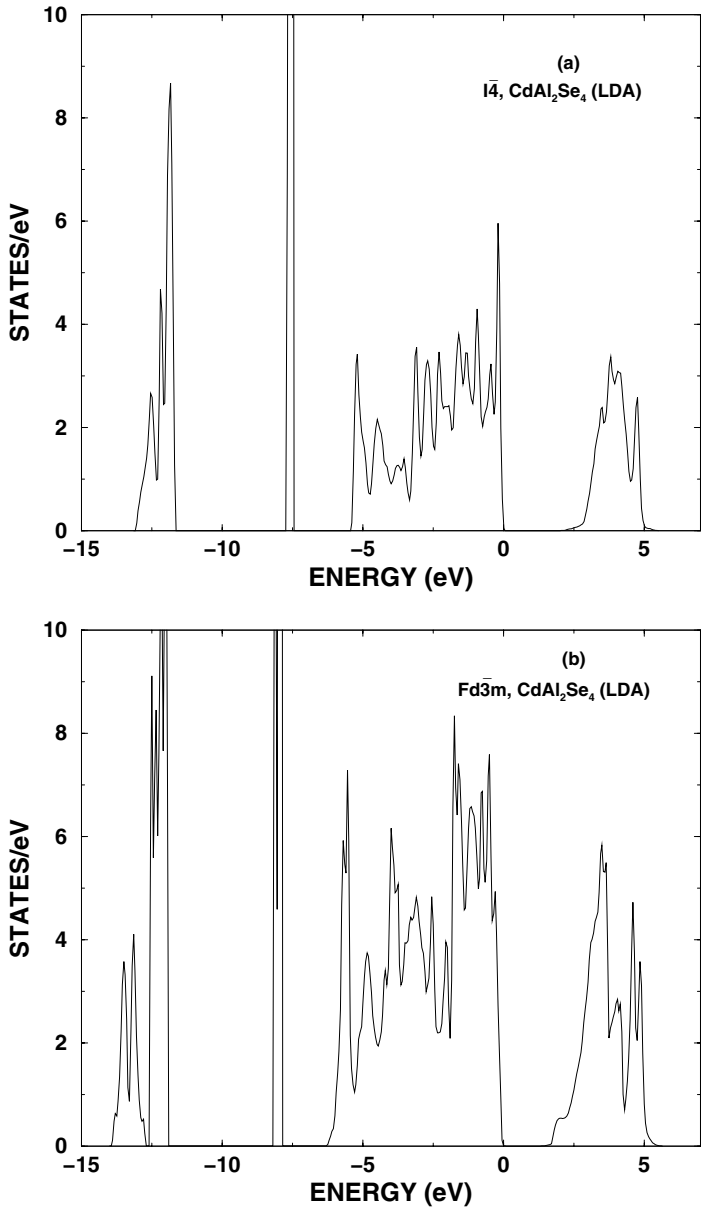

Figure 7. The LDA total electronic density of states of the equilibrium volumes V_0 of each phase (see table 2) obtained by a LDA calculation. The zero of the energies is at the top of the valence band. (a) The $I\bar{4}$ phase. (b) The spinel-like $Fd\bar{3}m$ phase.

Al(2c), and Se atoms, and in the directions $\vec{x}$ and $\vec{z}$ for the Cd atoms. The energy of each displaced configuration was obtained and the forces on the atoms were computed. The forces were divided by the corresponding finite displacement U_0 to give one complete row of the $\vec{k} = \vec{0}$ force-constant matrix. The entire force-constant matrix was calculated by applying symmetry operations to the independent rows. This method is exact, assuming the harmonic approximation. To avoid anharmonic terms, we have performed calculations with

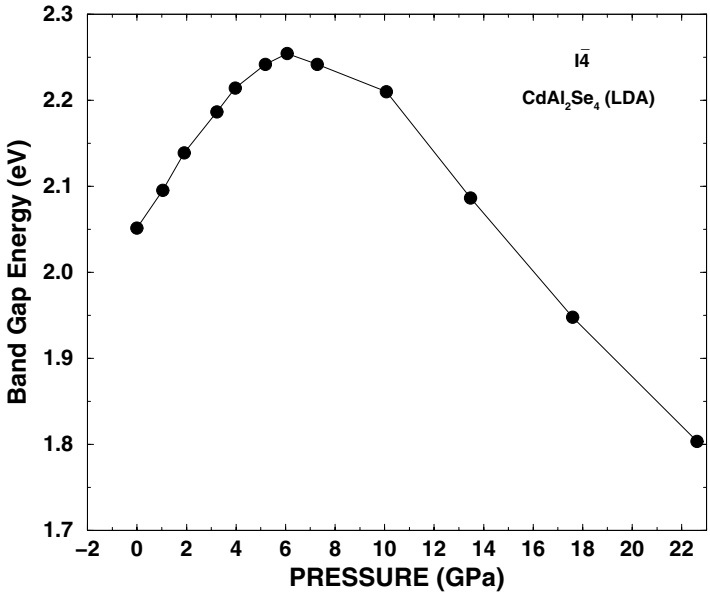

Figure 8. The pressure dependence of the LDA band gap of the geometrically LDA-optimized $I\bar{4}$ phase.

displacements of $+U_0$ and $-U_0$ and have averaged the force-constant matrix. The resultant force-constant matrix therefore contained an error that is fourth order in the displacements U_0.

The $I\bar{4}$ phase contains seven atoms per unit cell, which means that $(3 \times 7) - 3 = 18$ modes are optical. Group theory establishes [25] that the 18 optical modes are in three distinct irreducible representations in the combination 3A + 5B + 5E. All of the modes (A, B, and E) are Raman active, while only the E and B modes are infrared active. The E modes are doubly degenerate.

The calculated Γ-point phonon modes at zero pressure of the $I\bar{4}$ phase are shown in table 4. Also in this table are the experimental results of reference [10]. We have not calculated the longitudinal and transverse components of the polar modes E and B since they require knowledge of the effective charges. It can be seen in table 4 that the agreement between theory and experiment is outstanding, with the discrepancy being typically less than 5%. Theory and experiment agree completely on the vibrational symmetry assignments.

The pressure dependence of the Γ-point phonon modes provides information about the dynamic stability of the material. We show the calculated pressure dependence of the Γ-point phonon spectra of the $I\bar{4}$ phase in figure 10. It is seen that the general behaviour of the $I\bar{4}$ modes with pressure can be grouped into two categories.

(i) Modes with frequencies that increase with pressure. These are the high-frequency modes (above 300 cm^{-1}) and all of the low-frequency modes (below 200 cm^{-1}) except the two lowest E modes and the second B mode.
(ii) Modes with frequencies that decrease with pressure. These are the two lowest E modes and the second B mode.

None of these modes approach zero frequency with pressure. Thus the Γ-point phonons show no sign of a dynamically unstable lattice and a transition to another lattice with lower symmetry. Therefore, according to our results it can be said that at least up to 23 GPa (the highest pressure studied here) the $I\bar{4}$ lattice of $CdAl_2Se_4$ is still dynamically stable.

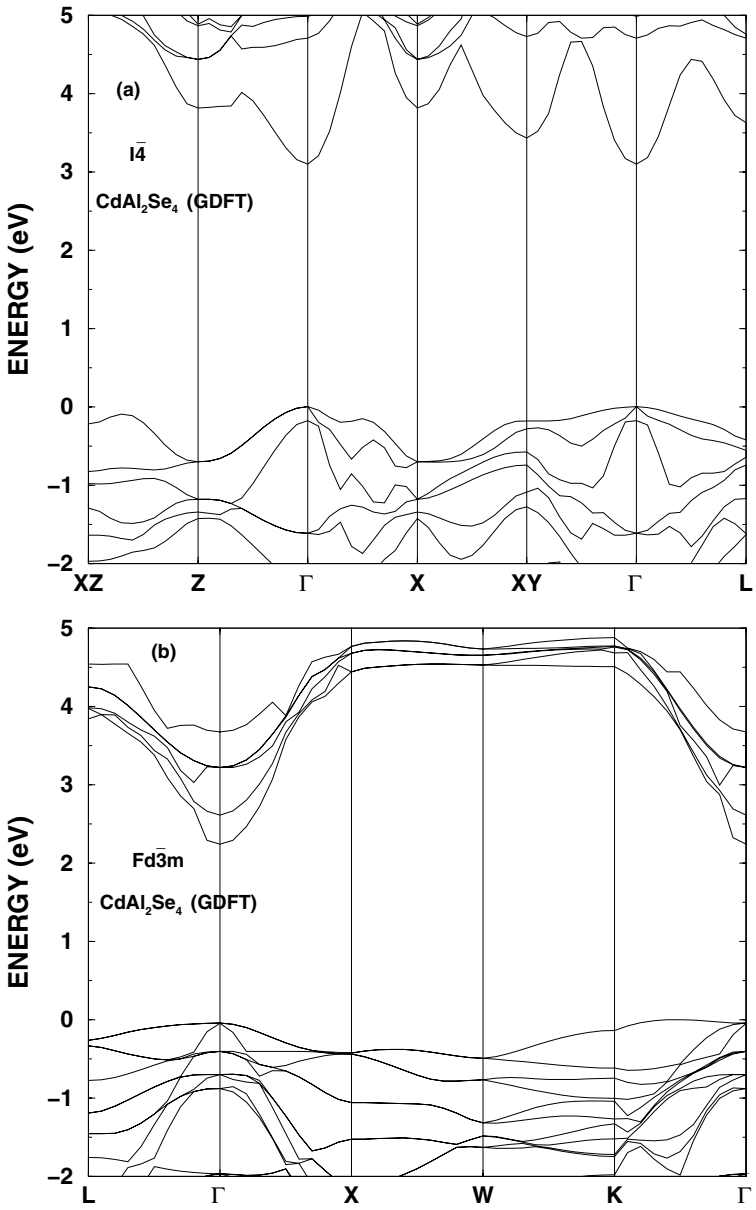

Figure 9. The GDFT-corrected near-band-gap electronic structure of the equilibrium volumes V_0 of each of the geometrically LDA-optimized phases. (a) The $I\bar{4}$ phase. (b) The spinel-like $Fd\bar{3}m$ phase.

There have been neither experimental nor theoretical studies on the pressure dependence of the vibrational spectra of $CdAl_2Se_4$. Recently, Ursaki *et al* [5] measured the Raman spectra of related materials, AGa_2X_4 (A = Cd, Zn; X = S, Se), under hydrostatic pressure. The $CdGa_2Se_4$ compound crystallizes in the $I\bar{4}$ phase and its vibrational spectrum has a pressure dependence very similar to that found here for $CdAl_2Se_4$. Ursaki *et al* [5] reported that $CdGa_2Se_4$ undergoes a disordering of the lattice as the pressure is increased. Such a disordering

Table 4. Γ-point ($\vec{k} = \vec{0}$) phonon modes of the geometrically LDA-optimized $I\bar{4}$ phase of $CdAl_2Se_4$: frequencies and symmetries. The experimental results correspond to those of Eifler *et al* [10] obtained at 300 °C. The experiment shows the TO–LO splitting in the polar modes E and B. We have not calculated the TO–LO splitting in these modes.

Theory				Experiment		
ω (cm^{-1})	Symmetry	Raman	IR	ω_{TO}	ω_{LO}	Symmetry
67.56	E	√	√	67.5	71	E
82.66	B	√	√	80	81.5	B
118.50	E	√	√	123.5	124	E
130.76	B	√	√	131.5	133.5	B
139.44	A	√		135.5		A
180.35	E	√		178	185	E
183.21	A	√		185		A
196.01	B	√	√	197	203	B
204.83	A	√		215		A
301.21	B	√	√	315	348	B
330.69	E	√	√	338.5	350.5	E
366.31	E	√	√	373	402	E
373.87	B	√	√	377.5	392.5	B

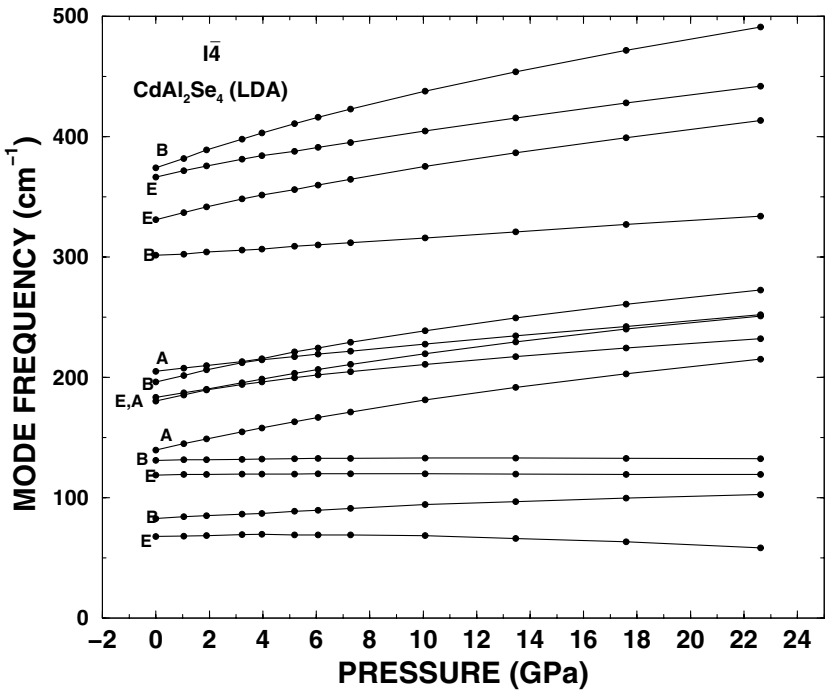

Figure 10. Vibrational spectra at $\vec{k} = \vec{0}$ of the geometrically LDA-optimized $I\bar{4}$ phase as a function of pressure. The symmetry of each mode is written beside the corresponding curve.

was divided into two stages, as predicted earlier by Bernard and Zunger [3]. In the first stage, the cations Cd and Ga become mixed and the $I\bar{4}$ symmetry changes to a disordered $I\bar{4}2m$ symmetry. In the second stage, the vacancies also become disordered and the $I\bar{4}2m$ phase becomes a disordered zinc-blende-like structure. In reference [5], the first stage of disordering

in $CdGa_2Se_4$ was related to the decrease with pressure of the lowest-frequency E mode. It is interesting to note that in figure 10 for $CdAl_2Se_4$, a slight decrease with pressure of the lowest-frequency E mode is also predicted. However, the $I\bar{4}$ phase considered here remains ordered.

5. Conclusions

We have used a first-principles electronic structure technique based on the density functional theory to study the stability, and electronic and vibrational properties of $CdAl_2Se_4$. The defective chalcopyrite-like phase $I\bar{4}$ and the spinel-like phase $Fd\bar{3}m$ have been considered. Our findings are summarized as follows.

(i) The generalized gradient approximation (GGA) is required to obtain the correct subtle energy relationship between the $I\bar{4}$ and the $Fd\bar{3}m$ phases of $CdAl_2Se_4$. The local density approximation (LDA) shows the $I\bar{4}$ and the $Fd\bar{3}m$ phases to have virtually the same energy, while in the GGA the $I\bar{4}$ phase is more stable, in agreement with experiments. With the GGA, the $Fd\bar{3}m$ phase is a high-pressure phase that appears at 3 GPa.

(ii) The generalized density functional theory (GDFT) is a valuable tool for correcting the underestimation in the LDA band gaps of defective-tetrahedral compounds. We find that the $I\bar{4}$ phase has a LDA band gap of 2.05 eV that opens up to 3.1 eV using the GDFT, in excellent agreement with experiment (2.95 eV). Both the LDA and the GDFT agree that the band gap is direct and at the Γ point. The spinel-like $Fd\bar{3}m$ phase band gap also opens up with GDFT. With LDA we obtained 1.47 eV, while with GDFT we obtain 2.28 eV. In both cases, the band gap is indirect. There are no experimental results for this phase.

(iii) The calculated pressure dependence of the Γ-point phonon spectra of the $I\bar{4}$ phase shows that no modes reach zero frequency up to 23 GPa. The agreement of the theoretical vibrational mode frequencies with experiment is outstanding.

Acknowledgments

MFC acknowledges funding by a Fulbright Fellowship from the Spanish Ministry of Education and Culture. We also acknowledge the NSF (DMR-99-86706). We would like to thank M Meléndez-Lira and Jianjun Dong for many insightful discussions that we had in the course of this work.

References

[1] Parthé E 1964 *Crystal Chemistry of Tetrahedral Structures* (New York: Gordon and Breach)
[2] Pamplin B R 1960 *Nature* **188** 136
[3] Bernard J E and Zunger A 1988 *Phys. Rev.* B **37** 6835
[4] Marinelli M, de Pascale T M, Meloni F, Mula G, Serra M and Baroni S 1989 *Phys. Rev.* B **40** 1725
[5] Ursaki V V, Burlakov I I, Tiginyanu I M, Raptis Y S, Anastassakis E and Anedda A 1999 *Phys. Rev.* B **59** 257
[6] Hahn H, Franck G, Kligler W and Storger A D 1955 *Z. Anorg. Allg. Chem.* **279** 241
[7] Range K J, Becker W and Weiss A 1968 *Z. Naturf.* b **23** 1261
[8] Krauss G, Krämer V, Eifler A, Riede V and Wenger S 1997 *Cryst. Res. Technol.* **32** 223
[9] Hecht D-D, Eifler A, Riede V, Schubert M, Krauß G and Krämer V 1998 *Phys. Rev.* B **57** 7037
[10] Eifler A, Hecht J-D, Riede V, Lippold G, Schmitz W, Krauß W, Krämer V and Grill W 1999 *J. Phys.: Condens. Matter* **11** 4821
[11] Eifler A, Hecht J-D, Lippold G, Riede V, Grill W, Krauß G and Krämer V 1999 *Physica* B **263+264** 806
[12] The Vienna *Ab Initio* Simulation Program (VASP) developed at the Institut für Theoretiche Physik of the Technische Universität Wien:

Kresse G and Furthmüller J 1996 *Comput. Mater. Sci.* **6** 15
[13] Vanderbilt D 1990 *Phys. Rev.* B **41** 7892
[14] Kresse G and Hafner J 1993 *Phys. Rev.* B **47** 558
Kresse G and Furthmüller J J 1996 *Phys. Rev.* B **55** 11 169
[15] Ceperley D M and Alder B J 1980 *Phys. Rev. Lett.* **45** 566
[16] Perdew J and Zunger A 1981 *Phys. Rev.* B **23** 5048
[17] Perdew J P 1991 *Electron Structure of Solids* ed P Ziesche and H Eschrig (Berlin: Akademie) p 11
[18] Monkhorst H J and Pack J D 1976 *Phys. Rev.* B **13** 5189
[19] Birch F 1952 *J. Geophys. Res.* **57** 227
[20] Fritsche L and Gu Y M 1993 *Phys. Rev.* B **48** 4250
[21] Remediaki I N and Kaxiras E 1999 *Phys. Rev.* B **59** 5536
[22] Dong J, Sankey O F, Deb K S, Wolf G and McMillan P F 2000 *Phys. Rev.* B **61** 11 979
[23] Dong J, Sankey O F and Kern G 1999 *Phys. Rev.* B **60** 950
[24] Dong J and Sankey O F 1999 *J. Phys.: Condens. Matter* **11** 6129
[25] Fateley W G, Dollis F R, McDevitt N T and Bently F F 1972 *Infrared and Raman Selection Rules for Molecular and Lattice Vibrations: the Correlation Method* (London: Wiley)